EMG Signal Enhancement via Multi-Objective Optimization of Hankel-Based Bayesian Learning

Salvador Echeveste * **Chunming Yang** **
Pranav A. Bhounsule ***

* *Department of Mechanical and Industrial Engineering, University of Illinois Chicago, Chicago, USA (e-mail: sechev6@uic.edu).*
** *Department of Mechanical and Industrial Engineering, University of Illinois Chicago, Chicago, USA (e-mail: jyang241@uic.edu).*
*** *Department of Mechanical and Industrial Engineering, University of Illinois Chicago, Chicago, USA (e-mail: pranav@uic.edu).*

Abstract: Electromyography (EMG) signals are essential for neuromuscular diagnosis and assistive device control but suffer from noise contamination that obscures clinically important transient features. We present an interpretable, automated framework that enhances EMG quality by integrating low rank Hankel matrix reconstruction with Bayesian regularized Koopman regression and optimized smoothing, all tuned through multi objective Bayesian optimization (MOBO). Raw EMG traces are embedded in a time delay Hankel matrix and decomposed via truncated singular value decomposition (SVD) to isolate underlying dynamics. A ridge regularized Bayesian regression learns a predictive transition operator, whose forecasts are optimally combined with the reconstructed signal. A windowed Makima median smoother provides final refinement. Key hyperparameters including embedding dimension, SVD rank, regularization variances, and fusion weight are selected to simultaneously maximize signal to noise ratio (SNR) and structural fidelity using Gaussian process surrogates and an expected hypervolume improvement (EHVI) criterion. When evaluated on walking and squatting EMG data from ten healthy adults across four muscle groups, our method achieves a 108.7% increase in a squared geometric mean (SGM) metric ($p = 0.0282$) and an 11.4% gain in normalized joint fidelity ($p = 0.0011$), while decoupling noise reduction from signal preservation (Pearson $r \approx 0$). These results establish a powerful, generalizable approach for real time clinical and rehabilitation applications.

Keywords: Bayesian optimization, Electromyography, Gaussian process regression, Hankel matrix decomposition, Multi-objective optimization

1. INTRODUCTION

Effective EMG signal processing is critical in rehabilitation, enabling accurate interpretation of muscle activation patterns that underpin neuromuscular diagnosis, patient monitoring, and assistive device control (Al-Ayyad et al., 2023; Toepp et al., 2023). Despite the availability of powerful tools, most standard filtering methods assume linearity and static noise. These methods rely on manual parameter tuning to improve signal-to-noise ratio (SNR) and often suppress transient components that are vital for clinical insight (Farago et al., 2022; Leone et al., 2025; Li et al., 2022).

Researchers employ more advanced denoising techniques to overcome these limitations, including enhanced wavelet thresholding (Ouyang et al., 2023; Lu et al., 2024), adaptive empirical mode decomposition variants (Xiao et al., 2019), and deep learning models (Ling et al., 2025). While these approaches boost SNR and better preserve intricate features, they frequently function as "black boxes" or demand extensive noise modeling—and still attenuate subtle but clinically relevant signal content (Zheng et al., 2022; Farago et al., 2022).

Techniques leveraging low-rank Hankel-matrix representations, such as Singular Spectrum Analysis (SSA) and the Cadzow algorithm, open new avenues for separating physiologically meaningful patterns from interference (Gillard and Usevich, 2022; Wadekar et al., 2022). The HAVOK framework, rooted in Koopman operator theory, extends this idea via time-delay embeddings to decompose data into interpretable transient and nonlinear modes (Brunton et al., 2017). However, its performance hinges critically on parameter choices, reintroducing the familiar balance between noise suppression and signal fidelity.

⋆ Sponsor and financial support acknowledgment goes here.

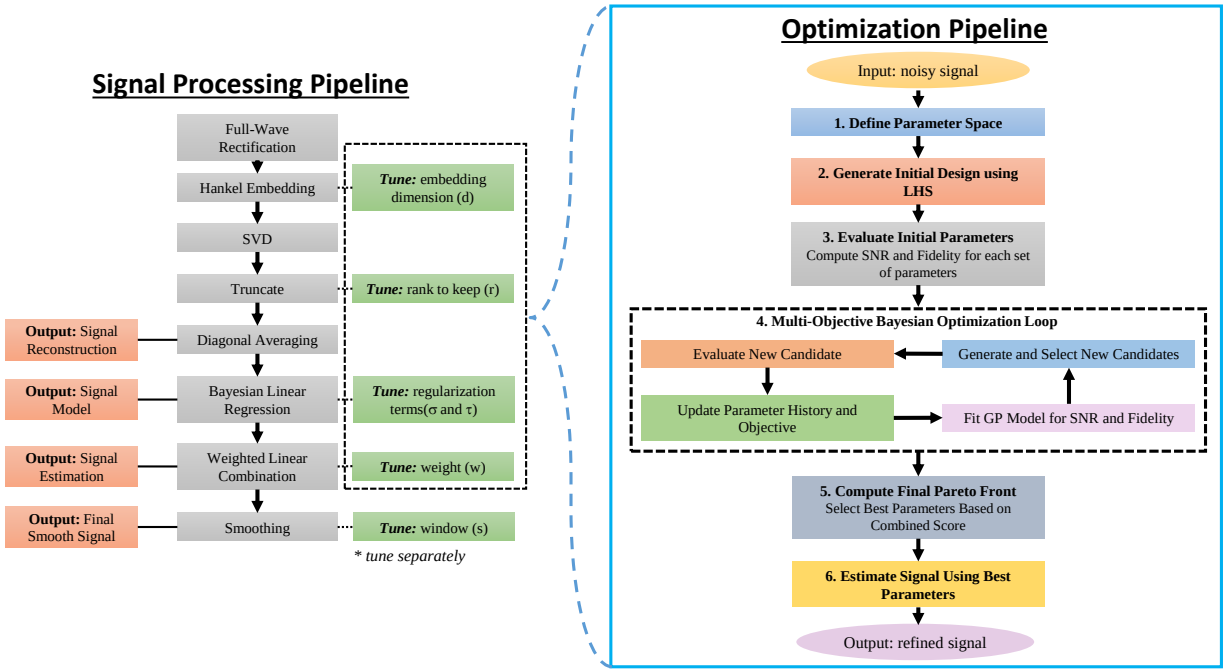

Fig. 1. Schematic of the EMG enhancement and optimization workflow. Raw EMG is denoised via an optimized process involving Hankel-SVD, prediction by a Bayesian Koopman model, weighted combination, and smoothing. The asterisk (*) indicates that the five parameters (d, r, σ, τ, w) are optimized via multi-objective Bayesian optimization, while the smoother window length (s) is optimized independently.

Most existing pipelines address tuning by hand or by optimizing a single objective, inevitably sacrificing true signal content along the way (Xiao et al., 2019; Ma et al., 2022; Bhaumik et al., 2023; Migon et al., 2023). Multi-objective Bayesian Optimization emerges to automate this trade-off, using probabilistic surrogate models to balance SNR, transient preservation, and computational cost (Yang et al., 2019; Morales-Hernández et al., 2024; Egele et al., 2023).

In this paper, we introduce a novel framework that couples Hankel-based dynamical decomposition with Bayesian -regularized linear regression and tunes parameters via (MOBO). Figure 1 provides a high-level overview of our entire EMG enhancement and optimization pipeline. To the best of our knowledge, the key novelties of our approach are:

- **Hankel-Bayesian signal modeling:** we combine low-rank Hankel-matrix reconstruction with Bayesian -regularized linear regression to achieve interpretable signal decomposition in the spirit of the HAVOK framework;
- **Pareto-optimal trade-off via MOBO:** we utilize MOBO to balance SNR improvement and signal fidelity as competing objectives, identifying a Pareto front rather than collapsing them into a single metric;
- **Robust smoothing filter:** we integrate windowed filtering, median filtering, and Makima interpolation to generate a smoothing filter that preserves transients while suppressing noise.

This integrated approach not only automates parameter tuning but also directly addresses the critical trade-off between noise suppression and retention of useful signal content—a challenge that remains unresolved in current EMG processing literature (Gómez-Verde et al., 2024; Gopal et al., 2022). In doing so, we extend established techniques from electroencephalography (EEG) and electrocardiogram (ECG) signal analysis to the domain of EMG, offering a comprehensive and interpretable solution for clinical practice.

2. METHODOLOGY

2.1 Data Acquisition

This study utilizes open-source biomechanical data (Scherpereel et al., 2023), which provide synchronized motion capture, ground-reaction forces, surface EMG (2 kHz sampling rate, Surface ElectroMyoGraphy for the Non-Invasive Assessment of Muscles (SENIAM) electrode placement), and Inertial Measurement Unit (IMU) streams from 12 healthy adults performing various cyclic and acyclic activities. For this study, we select ten subjects based on EMG signal quality and focus on two activities: level-ground walking and body-weight squatting. We process EMG channels for the rectus femoris (RF), biceps femoris (BF), gluteus maximus (GM), and medial gastrocnemius (GN). Raw EMG traces undergo full-wave rectification before downstream analysis.

2.2 Hankel-based Signal Reconstruction

A noisy signal $x(t)$ with N samples is first embedded into a Hankel matrix of dimension d:

$$\mathbf{H} = \begin{bmatrix} x(1) & x(2) & \cdots & x(N-d+1) \\ x(2) & x(3) & \cdots & x(N-d+2) \\ \vdots & \vdots & \ddots & \vdots \\ x(d) & x(d+1) & \cdots & x(N) \end{bmatrix}, \quad (1)$$

where d is the embedding (lag) dimension which controls how many past samples are used for reconstruction.

Singular Value Decomposition (SVD) is then applied:

$$\mathbf{H} = \mathbf{U}\mathbf{\Sigma}\mathbf{V}^\top, \tag{2}$$

and a low-rank approximation is obtained by retaining the first r components:

$$\mathbf{H}_r = \mathbf{U}_r\mathbf{\Sigma}_r\mathbf{V}_r^\top. \tag{3}$$

Diagonal averaging (Hankelization) converts $\mathbf{H}_r$ back into a time-domain signal:

$$\hat{x}(k) = \frac{1}{n_k}\sum_{i+j=k+1}[\mathbf{H}_r]_{ij}, \quad k = 1,\ldots,N, \tag{4}$$

where n_k denotes the number of elements in the k-th anti-diagonal. The output $\hat{x}(t)$ is thus a denoised estimate of the original $x(t)$.

2.3 Regularized Estimation via Bayesian Linear Regression

To estimate a robust model of the signal, we employ a Bayesian linear regression framework using two time-shifted Hankel matrices constructed from the state observations:

$$\mathbf{H}_1 = \mathbf{H}(:, 1{:}N{-}1), \tag{5}$$

$$\mathbf{H}_2 = \mathbf{H}(:, 2{:}N), \tag{6}$$

These matrices represent sequential state pairs, where $\mathbf{H}_1$ contains the states at time t, and $\mathbf{H}_2$ contains the corresponding states at time $t+1$. The transition matrix $\mathbf{A}$ is estimated via ridge regression:

$$\mathbf{A} = \left(\mathbf{H}_1^\top\mathbf{H}_1 + \lambda\mathbf{I}\right)^{-1}\mathbf{H}_1^\top\mathbf{H}_2, \tag{7}$$

$$\lambda = \frac{\sigma^2}{\tau^2}, \tag{8}$$

where σ^2 is the observation noise variance and τ^2 is the prior variance on A; both will be tuned as part of our hyperparameter set θ. This formulation corresponds to Maximum A Posteriori (MAP) estimation under a Gaussian prior and noise model, controlling model complexity and stability.

By incorporating prior information through regularization, this approach mitigates overfitting and provides a principled probabilistic framework for estimating signal dynamics. A one-step temporal shift of the learned dynamics yields the predicted signal:

$$\hat{\mathbf{x}}_{\text{pred}}(t+1) = \mathbf{A}\,\hat{\mathbf{x}}(t). \tag{9}$$

2.4 Signal Fusion

Having obtained both a reconstructed signal $\hat{x}(t)$ and a predicted signal $\hat{x}_{\text{pred}}(t)$, we fuse these estimates to exploit their complementary strengths. The fusion combines the reconstruction accuracy of $\hat{x}(t)$ with the dynamical consistency of $\hat{x}_{\text{pred}}(t)$:

$$\hat{x}_{\text{final}}(t) = w\,\hat{x}(t) + (1-w)\,\hat{x}_{\text{pred}}(t),$$

where $w \in [0,1]$ adjusts the balance between the two. We tune five key parameters to optimize performance:

$$\theta = \{\, d,\ r,\ \sigma^2,\ \tau^2,\ w\},$$

where d is the embedding dimension, r the SVD rank, σ^2 and τ^2 are regularization variances, and w the fusion weight. These parameters are selected via multiobjective Bayesian optimization (Section 2.5).

2.5 Multi-objective Bayesian Optimization

To identify the best parameter set θ, we apply Bayesian optimization with two objectives. These parameters affect both the Hankel reconstruction and the prediction model. Specifically, we consider:

- Embedding dimension d in $[50, 150]$,
- SVD rank r in $[3, 10]$,
- Regularization variances σ^2 in $[0.0001, 0.01]$ and τ^2 in $[0.1, 10]$,
- Fusion weight w in $[0, 1]$.

We begin by sampling candidate sets via Latin hypercube sampling to ensure each parameter is sampled evenly across its range. Each candidate is then evaluated on two metrics:

(1) **Signal to Noise Ratio (SNR).** For each nonoverlapping window i with mean μ_i and standard deviation σ_i,

$$\text{SNR}_i = 10\log_{10}\!\left(\tfrac{\mu_i^2}{\sigma_i^2+\epsilon}\right), \quad \text{SNR} = \frac{1}{N_{\text{win}}}\sum_{i=1}^{N_{\text{win}}}\text{SNR}_i, \tag{10}$$

where $\epsilon = 10^{-8}$ avoids division by zero.

(2) **Structural Similiarity Index Metric (SSIM) Fidelity.** We compute the structural similarity between reconstructed and original (unprocessed) windows:

$$\text{SSIM}(x,y) = \frac{(2\mu_x\mu_y + C_1)(2\sigma_{xy} + C_2)}{(\mu_x^2 + \mu_y^2 + C_1)(\sigma_x^2 + \sigma_y^2 + C_2)}, \tag{11}$$

where $C_1 = (0.01L)^2$ and $C_2 = (0.03L)^2$ with L being the dynamic range of values.

We fit Gaussian process surrogates to both objectives and use an expected hypervolume improvement (EHVI) criterion to propose new candidates. EHVI quantifies the expected improvement in the hyper-volume of the Pareto front, enabling efficient exploration of the multi-objective space. From the surrogate predictions, we extract the Pareto front of non-dominated solutions. The final parameter set is chosen by summing each candidate's normalized SNR and SSIM scores.

2.6 Windowed Makima Median Smoother

To further target any high-frequency noise artifacts and improve signal continuity we apply a post estimation smoothing stage. Starting from the estimated signal $\hat{x}(t)$ we divide it into M non overlapping windows of length s. For each window i we compute the median

$$m_i = \text{median}\big(\hat{x}(t)\big) \tag{12}$$

and define the window center

$$c_i = \frac{t_{\text{start}} + t_{\text{end}}}{2}. \tag{13}$$

We then reconstruct a continuous, smoothed signal by applying Makima (Modified Akima) interpolation to the set of points $\{(c_i, m_i)\}$, with extrapolation enabled at the edges:

$$\hat{x}_{\text{smooth}}(t) \;=\; \text{makima}\big(\{c_i\},\{m_i\},t\big). \tag{14}$$

To select the optimal window length s^* we use Bayesian optimization with a loss function that penalizes excessive fluctuations. For each candidate s we compute

$$\mathcal{L}(w) = \frac{\sum_t \left(\frac{d\hat{x}_{\text{smooth}}}{dt}\right)^2}{\sum_t \left(\frac{d^2\hat{x}_{\text{smooth}}}{dt^2}\right)^2 + \epsilon}, \tag{15}$$

where $\epsilon = 10^{-6}$ ensures numerical stability. This formulation promotes smooth changes while preserving curvature. We search s in $[25, 500]$ samples using an expected improvement criterion. The smoothed signal for s^* is retained for downstream analysis.

The full signal-processing sequence for one EMG channel is illustrated in Figure 2.

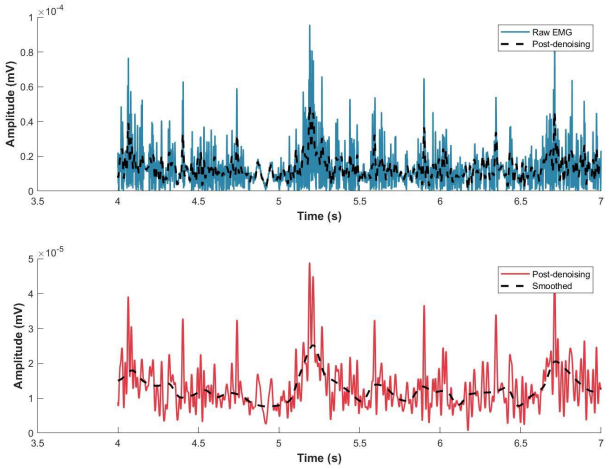

Fig. 2. Processing stages for one EMG channel. Top: raw signal to fused output (dashed). Bottom: fused output to Makima-median smoothing. Note that the fused output retains physiological features while reducing noise, and the final smoothing removes residual high-frequency artifacts.

2.7 Evaluation

To evaluate our proposed framework, we compare it against a control method representing standard EMG processing practices. The control pipeline consists of: (1) fourth-order Butterworth bandpass filter (20-450 Hz), (2) full-wave rectification, and (3) moving average smoothing with a 50 ms window. This approach is widely used in clinical and research settings (Merletti and Parker, 2004) and serves as our baseline for performance comparison.

We extract two complementary quantitative metrics to capture structural relevance and perceptual accuracy. We assess structural quality via $\text{SNR}_{\text{linear}}$ and perceptual fidelity via a structural similarity index. To guard against distortion from anomalous values we first remove outliers using a median based nearest neighbor interpolation with a window width of 5 samples. These outliers typically arise from motion artifacts or electrode displacement during data collection.

To integrate these dimensions we employ two fusion strategies. First we define the Squared Geometric Mean (SGM) as the product of quality and fidelity:

$$\text{SGM} = \text{SNR}_{\text{linear}} \times \text{Fidelity} \tag{16}$$

$$\text{SNR}_{\text{linear}} = 10^{\text{SNR}/10} \tag{17}$$

This metric highlights cases where both measures are high. Second we normalize SNR and fidelity to the unit interval across all subjects over the full data set and define a joint metric as their sum:

$$\text{JointMetric} = \text{Norm}(\text{SNR}) + \text{Norm}(\text{Fidelity}). \tag{18}$$

This additive measure is invariant to scale and permits direct comparison across groups. By pairing a multiplicative metric that rewards simultaneous excellence with an additive normalized metric we achieve a robust evaluation framework.

Stratified Analysis by Activity and Muscle We further analyze performance by activity and by muscle group. We compare walking and squatting alongside four muscle groups: Rectus Femoris, Biceps Femoris, Gastrocnemius and Gluteus Maximus. This stratification reveals task specific and muscle specific trends that may be masked in aggregate results. The approach supports deeper insight for biomechanics and clinical applications.

Statistical Analysis We evaluate differences between control and experimental groups using paired two-sample t-tests on both SGM and the joint metric. To assess whether structural quality and perceptual fidelity vary independently we compute Pearson correlation coefficients within each group. These correlations indicate the degree of coupling between the two metrics.

3. RESULTS

The proposed method exhibits an average improved fidelity retention of .571 relative to the control method, while the raw SNR metric actually shows a decrease of 6 dB. Despite the SNR decrease, these values translate into a combined SGM improvement of 108.7% (p = 0.0282) and a normalized joint metric gain of 11.4% (p = 0.0011), indicating superior performance to traditional methods by successfully mitigating the trade-off between noise suppression and preservation of critical signal features. Figure 4 shows the comparison of the two metrics between the control group and the experimental group.

The correlation analysis showed a Pearson's value of r = -0.6421 for the control group and r=0.011 for the experimental group. Figure 3 presents scatter plots of SNR versus fidelity with regression lines.

For Walking (Activity 1), the combined metric (SGM) increased by 56.8% relative to control ($p = 0.327$), and the normalized joint metric increased by 16.0% ($p < 0.001$). For Squatting (Activity 2), the SGM increase was 157.9% ($p = 0.0472$) and the joint metric increased by 7.10% ($p = 0.18$). Figure 6 presents the SGM and joint-metric results separately for walking and squatting.

In the RF, the SGM metric increased by 214.0% ($p < .001$), while the normalized joint metric increased by 32.8% ($p < .001$). In the BF, SGM decreased by 84.2% ($p < .001$ and the joint metric decreased by 18.9% ($p < .001$). For the GN, the SGM change was -15.0% ($p = 0.379$) with a joint metric increase of 7.10% ($p = 0.0698$). Finally, in the GM, SGM increased by 332.2} ($p = 0.00275$) while the joint metric increased by 36.3% ($p < .001$). Figure 5 shows SGM and joint-metric comparisons for each muscle group (RF, BF, GN, GM).

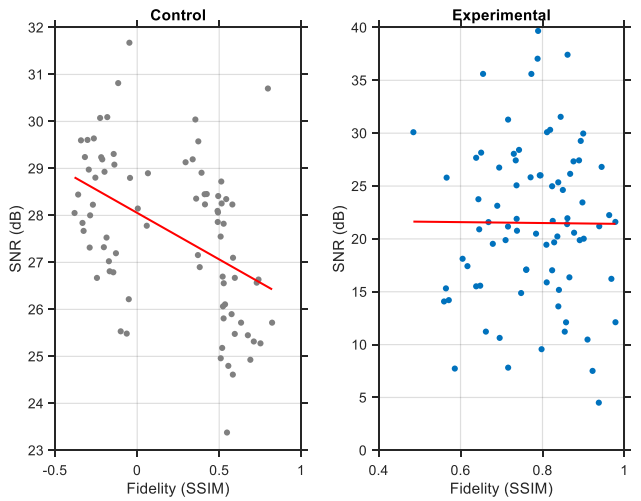

Fig. 3. Scatter of SNR vs. SSIM for control (gray) and our method (blue). Dashed red lines are linear fits showing strong negative correlation in control (r=–0.64) versus near zero in our pipeline (r=0.01).

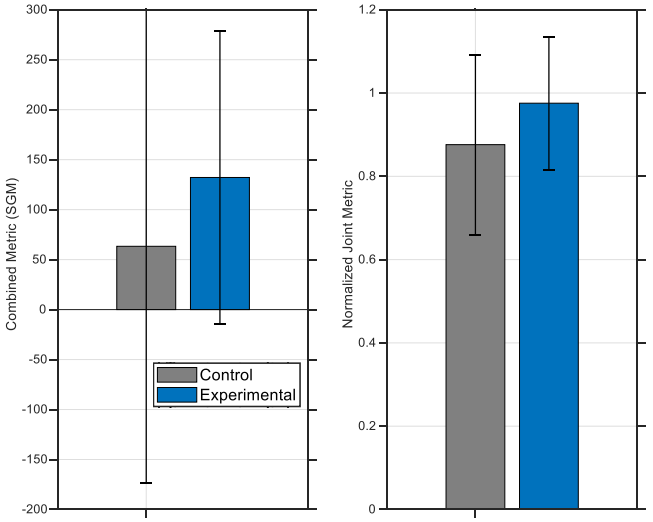

Fig. 4. Mean and standard deviation comparison of control (gray) and experimental (blue) on SGM (left) and normalized joint metric (right) across all subjects and activities. Control refers to the standard EMG processing pipeline, while Experimental refers to our proposed Hankel-Bayesian optimization framework.

4. DISCUSSION

The results demonstrate that our multi-objective optimization framework strikes a superior balance between noise suppression and signal fidelity. Although the raw SNR decreases by 6dB relative to the control method, fidelity retention improves markedly by 0.571. When these two effects combine into the SGM, we observe a 108.7% gain (p=0.0282), and the normalized joint metric increases by 11.4% (p=0.0011). These outcomes confirm that optimizing multiple objectives yields more clinically meaningful reconstructions than single-objective tuning.

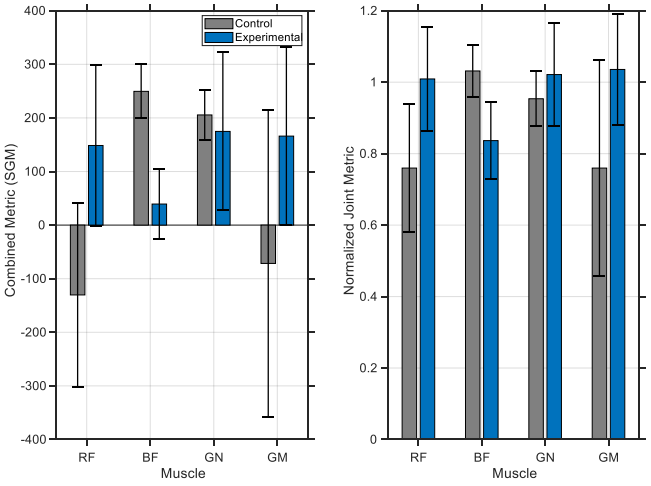

Fig. 5. Muscle-specific mean±standard deviation for control (gray) and experimental (blue) on SGM (left) and joint metric (right) for RF: rectus femoris, BF: biceps femoris, GN: gastrocnemius, and GM: gluteus maximus

.

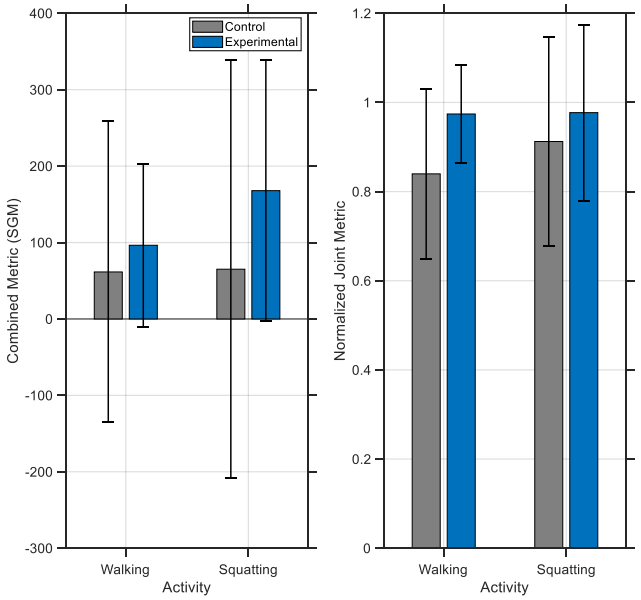

Fig. 6. Activity-specific mean and standard deviation for walking and squatting, comparing control and experimental methods on SGM (left) and joint metric (right).

The correlation analysis further underscores this benefit. In the control pipeline, SNR and fidelity exhibit a strong negative correlation (r=–0.6421), indicating that gains in noise reduction come at the expense of true signal content. By contrast, the Pearson coefficient for our method is essentially zero (r=0.011), showing that the two goals decouple effectively. This decoupling validates our use of Pareto-optimal trade-offs rather than a single composite criterion.

When stratified by activity, the framework delivers consistent improvements in both walking and squatting. For

level-ground walking, the SGM rises by 56.8% (p=0.327) and the normalized joint metric by 16.0% (p<.001). In body-weight squatting, the SGM increases even more steeply by 157.9% (p=0.0472), with a 7.1% rise in the joint metric (p=0.186). These patterns suggest that our method proves particularly effective for higher-amplitude or more nonlinear movements, where transient features are critical.

Despite these positive outcomes, some limitations remain. We use healthy adult data and offline analysis; real-time performance on pathological signals must be evaluated. The computational cost of Bayesian optimization is non-trivial, and simplifying surrogate models could accelerate deployment. Finally, larger and more diverse cohorts are required to confirm generalizability.

5. CONCLUSIONS

We introduce an automated EMG denoising framework coupling Hankel decomposition, Bayesian-regularized Koopman regression, Makima smoothing, and EHVI-driven Gaussian-Process multi-objective optimization. It achieves 108.7% SGM and 11.4% joint-metric gains (p<0.05), decoupled SNR–fidelity ($r \approx 0$), and task-/muscle-specific enhancements. This interpretable approach supports future real-time clinical and assistive-device applications.

REFERENCES

Al-Ayyad, M., Owida, H.A., De Fazio, R., Al-Naami, B., and Visconti, P. (2023). Electromyography monitoring systems in rehabilitation: A review of clinical applications, wearable devices and signal acquisition methodologies. *Electronics*, 12(7), 1520.

Bhaumik, D.K., Wang, Y., Yen, P.S., and Ajilore, O.A. (2023). Development of a bayesian multimodal model to detect biomarkers in neuroimaging studies. *Frontiers in Neuroimaging*, 2, 1147508.

Brunton, S.L., Brunton, B.W., Proctor, J.L., Kaiser, E., and Kutz, J.N. (2017). Chaos as an intermittently forced linear system. *Nature communications*, 8(1), 19.

Egele, R., Chang, T., Sun, Y., Vishwanath, V., and Balaprakash, P. (2023). Parallel multi-objective hyperparameter optimization with uniform normalization and bounded objectives. *arXiv preprint arXiv:2309.14936*.

Farago, E., MacIsaac, D., Suk, M., and Chan, A.D. (2022). A review of techniques for surface electromyography signal quality analysis. *IEEE Reviews in Biomedical Engineering*, 16, 472–486.

Gillard, J. and Usevich, K. (2022). Hankel low-rank approximation and completion in time series analysis and forecasting: a brief review. *arXiv preprint arXiv:2206.05103*.

Gómez-Verde, D., Esteban-Romero, S., Gil-Martín, M., and San-Segundo, R. (2024). Gesture recognition using electromyography and deep learning. *Engineering Proceedings*, 82(1), 38.

Gopal, P., Gesta, A., and Mohebbi, A. (2022). A systematic study on electromyography-based hand gesture recognition for assistive robots using deep learning and machine learning models. *Sensors*, 22(10), 3650.

Leone, A., Carluccio, A.M., Caroppo, A., Manni, A., and Rescio, G. (2025). A systematic review of surface electromyography in sarcopenia: Muscles involved, signal processing techniques, significant features, and artificial intelligence approaches. *Sensors*, 25(7), 2122.

Li, Y., Su, Z., Chen, K., Zhang, W., and Du, M. (2022). Application of an emg interference filtering method to dynamic ecgs based on an adaptive wavelet-wiener filter and adaptive moving average filter. *Biomedical Signal Processing and Control*, 72, 103344.

Ling, L., Wei, L., Feng, B., Yu, Z., and Wang, L. (2025). semg-based knee angle prediction: An efficient framework with xgboost feature selection and multi-attention lstm. *IEEE Sensors Journal*.

Lu, J., Li, L., Gong, Y., Liu, X., Zhang, F., and Zhu, B. (2024). Experimental and numerical investigations of the noise induced by cavitation in a centrifugal pump. *Iranian Journal of Science and Technology, Transactions of Mechanical Engineering*, 48(4), 1937–1955.

Ma, J., Li, H., Tang, B., Wang, J., Zou, Z., and Zhang, M. (2022). Rolling bearing fault diagnosis based on improved vmd-adaptive wavelet threshold joint noise reduction. *Advances in Mechanical Engineering*, 14(10), 16878132221128397.

Merletti, R. and Parker, P.J. (2004). *Electromyography: physiology, engineering, and non-invasive applications*. John Wiley & Sons.

Migon, H.S., Alves, M.B., Menezes, A.F., and Pinheiro, E.G. (2023). A review of bayesian dynamic forecasting models: Applications in marketing. *Applied Stochastic Models in Business and Industry*, 39(3), 471–493.

Morales-Hernández, A., Rojas Gonzalez, S., Van Nieuwenhuyse, I., Couckuyt, I., Jordens, J., Witters, M., and Van Doninck, B. (2024). Bayesian multi-objective optimization of process design parameters in constrained settings with noise: an engineering design application. *Engineering with Computers*, 40(4), 2497–2511.

Ouyang, C., Cai, L., Liu, B., and Zhang, T. (2023). An improved wavelet threshold denoising approach for surface electromyography signal. *EURASIP Journal on Advances in Signal Processing*, 2023(1), 108.

Scherpereel, K., Molinaro, D., Inan, O., Shepherd, M., and Young, A. (2023). A human lower-limb biomechanics and wearable sensors dataset during cyclic and non-cyclic activities. *Scientific Data*, 10(1), 924.

Toepp, S.L., Mohrenschildt, M.V., and Nelson, A.J. (2023). An emg-based biofeedback system for tailored interventions involving distributed muscles. *IEEE Sensors Journal*, 23(22), 28095–28109.

Wadekar, S., Mahalkari, A., Ali, A., and Gupta, A. (2022). A review on singular spectrum analysis. In *2022 IEEE International Conference on Current Development in Engineering and Technology (CCET)*, 1–6. IEEE.

Xiao, F., Yang, D., Guo, X., and Wang, Y. (2019). Vmd-based denoising methods for surface electromyography signals. *Journal of Neural Engineering*, 16(5), 056017.

Yang, K., Emmerich, M., Deutz, A., and Bäck, T. (2019). Multi-objective bayesian global optimization using expected hypervolume improvement gradient. *Swarm and evolutionary computation*, 44, 945–956.

Zheng, Z., Wu, Z., Zhao, R., Ni, Y., Jing, X., and Gao, S. (2022). A review of emg-, fmg-, and eit-based biosensors and relevant human–machine interactivities and biomedical applications. *Biosensors*, 12(7), 516.